nanomaterials

MDPI

Article

Prediction of Thermo-Physical Properties of TiO_2-Al_2O_3/Water Nanoparticles by Using Artificial Neural Network

Milad Sadeghzadeh [1], Heydar Maddah [2], Mohammad Hossein Ahmadi [3,*], Amirhosein Khadang [2], Mahyar Ghazvini [4], Amirhosein Mosavi [5,6,7,8,*] and Narjes Nabipour [9,*]

1 Department of Renewable Energy and Environmental Engineering, University of Tehran, Tehran 1439957131, Iran; milad.sadeghzadeh@gmail.com
2 Department of Chemistry, Payame Noor University (PNU), Tehran P.O. Box, 19395-3697, Iran; heydar.maddah@gmail.com (H.M.); Amirhossein.khadang77@gmail.com (A.K.)
3 Faculty of Mechanical Engineering, Shahrood University of Technology, POB- Shahrood 3619995161, Iran
4 Department of Ocean and Mechanical Engineering, Florida Atlantic University, 777 Glades Road Boca Raton, FL 33431, USA; m.ghazvini@alumni.ut.ac.ir
5 Kalman Kando Faculty of Electrical Engineering, Obuda University, 1034 Budapest, Hungary
6 Institute of Structural Mechanics (ISM), Bauhaus-Universität Weimar, 99423 Weimar, Germany
7 Thuringian Institute of Sustainability and Climate Protection, 07743 Jena, Germany
8 Department of Mathematics and Informatics, J. Selye University, 94501 Komarno, Slovakia
9 Institute of Research and Development, Duy Tan University, Da Nang 550000, Viet Nam
* Correspondence: mohammadhosein.ahmadi@gmail.com or mhosein.ahmadi@shahroodut.ac.ir (M.H.A.); amir.mosavi@uni-weimar.de (A.M.); narjesnabipour@duytan.edu.vn (N.N.)

Received: 28 December 2019; Accepted: 29 March 2020; Published: 7 April 2020

Abstract: In this paper, an artificial neural network is implemented for the sake of predicting the thermal conductivity ratio of TiO_2-Al_2O_3/water nanofluid. TiO_2-Al_2O_3/water in the role of an innovative type of nanofluid was synthesized by the sol–gel method. The results indicated that 1.5 vol.% of nanofluids enhanced the thermal conductivity by up to 25%. It was shown that the heat transfer coefficient was linearly augmented with increasing nanoparticle concentration, but its variation with temperature was nonlinear. It should be noted that the increase in concentration may cause the particles to agglomerate, and then the thermal conductivity is reduced. The increase in temperature also increases the thermal conductivity, due to an increase in the Brownian motion and collision of particles. In this research, for the sake of predicting the thermal conductivity of TiO_2-Al_2O_3/water nanofluid based on volumetric concentration and temperature functions, an artificial neural network is implemented. In this way, for predicting thermal conductivity, SOM (self-organizing map) and BP-LM (Back Propagation-Levenberq-Marquardt) algorithms were used. Based on the results obtained, these algorithms can be considered as an exceptional tool for predicting thermal conductivity. Additionally, the correlation coefficient values were equal to 0.938 and 0.98 when implementing the SOM and BP-LM algorithms, respectively, which is highly acceptable.

Keywords: thermal conductivity; TiO_2-Al_2O_3/water; nanofluid; artificial neural network

1. Introduction

Recently, numerous endeavors have been made in order to enhance the performance of various applications with the help of nanotechnology [1–4]. As an illustration, it is practicable to reduce system size or enhance the thermal performance of materials [5–8]. In this way, some investigations have been implemented on the use of nanotechnology in thermal applications [9–19]. Additionally, some studies

have focused on the prediction of the thermal conductivity ratio associated with various nanofluids with the help of using experiments and artificial neural networks [20–31]. Vafaei et al. [32] predicted the thermal conductivity ratio of MgO-MWCNTs/EG hybrid nanofluids by using ANN (artificial neural network) at the temperature range of 25–50 °C. According to the results, the best performance belonged to the neural network with 12 neurons in the hidden layer. Also, an investigation has been carried out by Afrand et al. [33] to estimate the thermal conductivity of MgO/water nanofluid. Furthermore, by implementing an ANN, convective heat transfer of TiO_2/water nanofluid has been studied by Esfe et al. [34]. As indicated in the results, the regression coefficient of the model for the Nusselt number's data is 99.94%. Azizi et al. [35] employed ANN to estimate the water holdup in different layouts of oil-water two-phase flow. In another use of ANN, Azizi et al. [36] investigated the estimation of void fraction in pipes with different inclination. ANN-based methods have this potential to give high precision estimation which can be beneficial in real practice since the actual experiment is not only so expensive but also very time-consuming.

On the other hand, the sol–gel process involving hydrolysis and condensation reactions of alkali precursors is an appropriate method for the synthesis of ultra-fine metal oxide [37]. Different researchers have used the sol–gel method in different conditions. Li et al. [38] added tetra-n-butyl titanate to deionized water and hydrochloric acid or ammonia. After milling and drying the gel at different temperatures, TiO_2 nanopowder was obtained. Zhang et al. [39] used the sol–gel microemulsion method. They synthesized TiO_2 nanoparticles by hydrolysis of tetraizo titanium Prop Oxide with 80 Tween-Span in a microemulsion and then calcined it is at different temperatures. The results show that the particles are spherical. In some cases, the surfactant is used in the sol–gel process. Pavasupree et al. [40] synthesized semi-porous TiO_2 nanoparticles by adding hydrochloride clarinylamine (LAHC) as a surfactant to the precursor solution. The resulting powders were calcined for 4 h at 400 °C. In the same way, Colon et al. [41] increased the specific surface area of the particles by adding activated carbon to the solution. The XRD results showed only the presence of the anatase phase in the powders. Li et al. [37] aged the gel for 12 h at 100 °C after drying it. The results showed that aging help to remove organic compounds and influence atomic penetration and crystalline anatase. In 2014, SiO_2 nanoparticles were synthesized by Oliveira et al. They used the polypropylene matrix in their research. Their results showed that the production of inorganic nanoparticles in a polymer solution does not require solvent through the reaction in the molten phase [42]. Moreover, the influence of adding Al_2O_3 and TiO_2 nanoparticles into the drilling mud was studied by Ghasemi et al. [43]. The size of Al_2O_3 and TiO_2 nanoparticles were 20 and 60 nm, respectively, and a concentration of 0.05 wt. %. Based on the obtained results of temperature and pressure effects, the drilling mud rheological properties such as plastic viscosity are decreased by increasing the temperature, nonetheless, the pressure rise augments these properties. Additionally, the influences of pressure in low temperature outweighs in high temperatures. Also, the effective electrical conductivity of Al_2O_3 nanoparticles was experimentally measured by Ganguly et al. [44]. For examining the influences of temperature variations and volume fraction on the electrical conductivity of Al_2O_3 nanofluids, experiments have been carried out as a function of these parameters. As indicated in the results, the electrical conductivity increases significantly with augmenting volume fraction and temperature. Nonetheless, the effective conductivity's reliance on the volume fraction is much higher than the temperature. Furthermore, some investigations have been intensively carried out for increasing the nanofluids' thermal conductivity with the help of applying different kinds of nanoparticles [45,46].

The aim of this study is to investigate the thermo-physical properties of TiO_2-Al_2O_3 nanoparticles in water that can be employed as a coolant fluid with its improved thermal properties. This is accomplished by conducting experiments on various volumes of nanoparticles in water. In this study, special attention has been paid to the temperature effect on the nanofluid's thermal conductivity. The temperature's influence on the thermal conductivity of TiO_2 nanofluid has not been reported yet. Furthermore, the current investigation discloses the influence of temperature and nanoparticle concentrations on the thermal properties of hybrid nanofluids. With the help of the experimental results

obtained by this study, researchers can acquire exceptional information regarding the displacement of nanofluid and its properties, in which appropriate theoretical models can be achieved in the future.

2. Test section

Synthesis of TiO_2-Al_2O_3 Nanoparticles and Characterization

In this study, the sol–gel method was used to synthesize TiO_2-Al_2O_3 nanoparticles prepared in various percentages of Al_2O_3 (10–60). Two different solution samples were prepared for this nanofluid. In the first sample, 0.1105 mol (2 g) of $TiCl_4$ was dissolved in a solution that contains 10 mL of methyl acetate, 10 mL of ethanolamine and 100 mL of ethanol, and stirred for one hour at room temperature. Finally, a uniform suspension was produced. Then, $AlCl_3$ was added to the solution in various weights (0–100%) and the resulting solution was stirred for one hour at 80 °C. The second sample solution was made up of 30 mL of n-hexane, 20 mL of ethanol, 4 mL of methyl acetate and 5 mL of ammonium hydroxide. The second sample was added to the first sample and the solution was mixed simultaneously to obtain the hydrogel. By adding the second sample, the viscosity of the hydrogel increased. After the addition of the sample was complete, the solution was stirred at room temperature for 48 h and then kept at room temperature for 12 h. After 12 h, with the help of water, the obtained gel was washed to remove the chloride salts and then separated solids from it. The solids were washed three times with distilled water and then placed in an oven for 3 h at 900 °C. Figure 1 shows the schematic of nanocomposite synthesis.

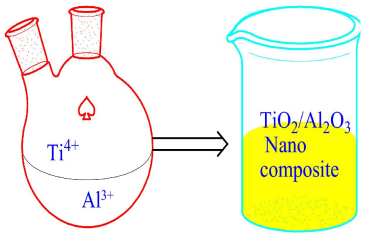

Figure 1. Schematic of nanocomposite synthesis.

The preparation of nanofluid is the first step in changing the heat transfer efficiency. The preparation of nanofluid by adding the nanoparticles to the base fluid should not be considered as a solid–liquid mixture. Because the preparation of nanofluid requires special conditions. Some of these special conditions include uniform and stable suspension, aggregation of particles and the lack of change in the nature of the base fluid. Different methods are used to achieve these specific properties. Various concentrations of nanofluids are prepared by using the equation below:

$$\varphi\ (Volume\ \text{concentration}\%) = \frac{\frac{w_{np}}{\rho_{np}}}{\frac{w_{np}}{\rho_{np}} + \frac{w_{water}}{\rho_{water}}} \quad (1)$$

where ρ_{np} and ρ_{water} represent the nanoparticles' density and water density, respectively. w is their mass [5].

Nanofluids that are prepared by the two-step method should be stable and the particle should not be sedimented in the fluid. Therefore, the nanofluid's stabilization should be considered.

In this study, a magnetic stirrer was used for nanofluid stability. The agitation intensity is crucially important for the nanoparticles' dispersion. The particles are connected to each other through bonds and the weak bonds are broken with force. However, there is a forceful propensity in nanoparticles for agglomerating because of the van der Waals force. We used the TEM analysis to evaluate the produced nanoparticles (Electro Microscopy) (PHILIPS EM 208, FEI, Hillsboro, Oregon, USA). SEM analysis was used to evaluate the morphology of synthesized nanoparticles. Figure 2 shows the SEM of pure nanoparticles and nanocomposites.

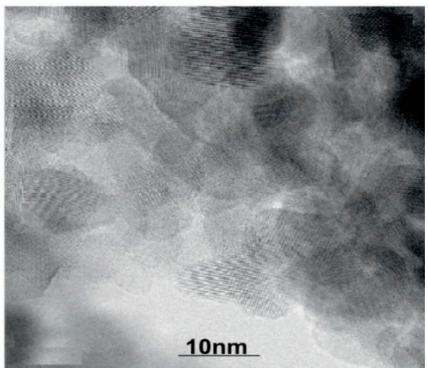

Figure 2. SEM images of nanoparticles after dispersion (20% alumina and 80% titanium).

According to the above, 20% alumina and 80% titanium were selected as samples for heat transfer analysis (the main objective of this study is to improve the properties of TiO_2). Therefore, adding more alumina will keep TiO_2 away from its main. With the help of the TCi Thermal Conductivity analyzer made by Canada's C-Therm, the thermal conductivity of the nanocomposite has been calculated experimentally. Also, the Brookfield Viscometer was used to measure the viscosity of prepared nanofluid. Based on the manufacturer and the obtained results, the proposed approach for measuring thermal conductivity brings an uncertainity of ±2% with the deviation of 4% for each measurement. The repeatability and accuracy of the viscometer used are ±0.2% and ±1% in the full-scale range (FSR) of measurements, respectively. One noteworthy approach in the field of thermal analysis is differential scanning calorimetry (DSC). This approach can be found in ASTM E1269. The ASTM E1269 is the standard defined procedure for measuring specific heat capacity through DSC approach. In this research, the improved modulated-DSC approach is used to obtain the specific heats. In modulated-DSC, a sinusoidal temperature fluctuation is employed instead of a linear ramp. This novel technique is capable to calculate the heat capacity and the heat flow of the samples, simultaneously.

3. Results and Discussion

As shown in Figure 3, the specific heat capacity of the nanocomposite varied linearly within the range 300–360 K. For temperatures of 300 K, the nanocomposite has a higher thermal capacity than its components. At this temperature, the nanocomposite's average heat capacity was 0.75 J/gK. In the range of 300–360 K, the average heat capacity was 0.78 J/gK. Since the temperature of the heat transfer analysis was mainly in this range, this number was chosen as the basis for our calculation.

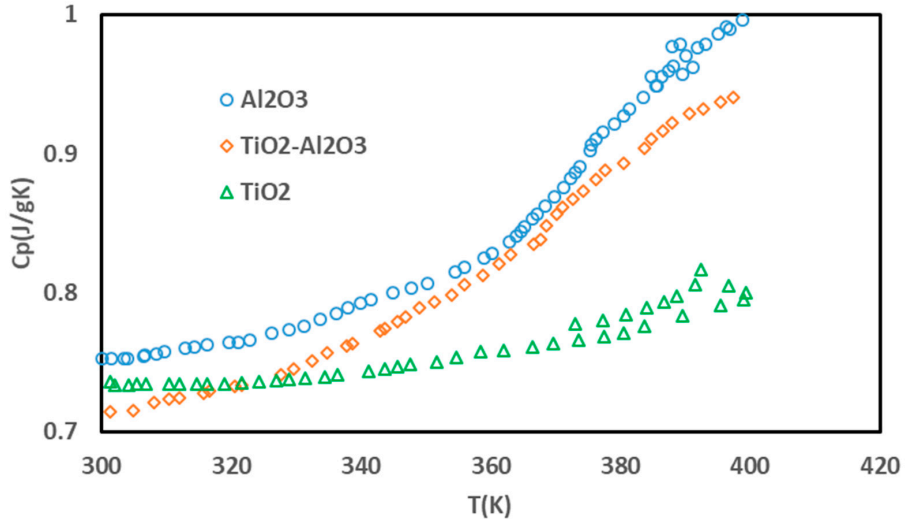

Figure 3. The results of the specific heat capacity of the nanocomposite.

Based on the results, it can be said that in the initial intervals, the thermal conductivity of the nanocomposite was within the range of its components. Because of the large number of Al_2O_3 particles in the nanocomposite, the thermal conductivity of the nanocomposite was very close to that of Al_2O_3. Based on Figure 4, the thermal conductivity coefficient was calculated to be 11.7 W/mK within the range of 300–360 K.

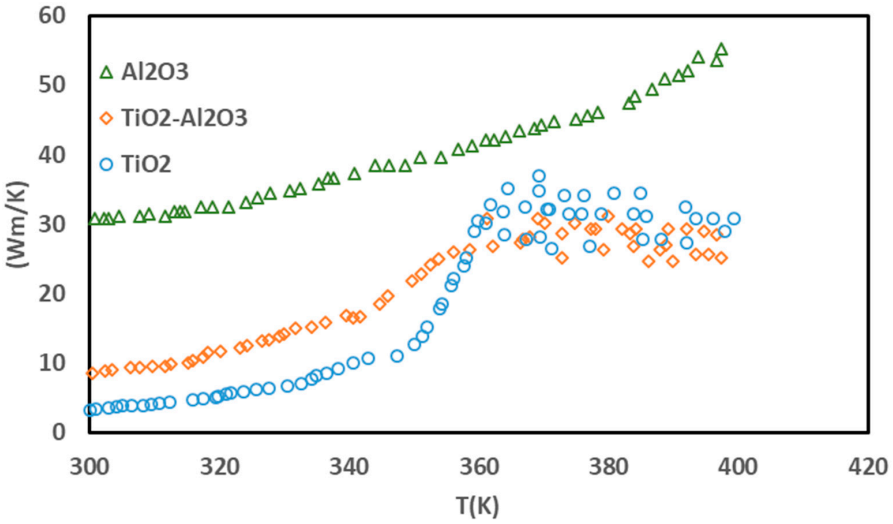

Figure 4. The results of the thermal conductivity coefficient of the nanocomposite.

The variations in the thermal conductivity of the nanofluid with respect to concentration are shown in Figure 5. According to Figure 5, with increasing nanofluid concentration, thermal conductivity also increased. It should be noted that overconcentration may be due to the agglomeration of particles and the reduction of the thermal conductivity of the nanofluid. Increasing the temperature leads to enhanced thermal conductivity. This is due to Brownian motion and an increase in the collision of the particles with each other. Since the presented equations are not based on nanocomposite in nanofluid, or the base fluid is not combined, it is not possible to match the data with this equation. Here, the experimentally measured data is fit on the basis of temperature and concentrations to be employed in heat transfer analysis.

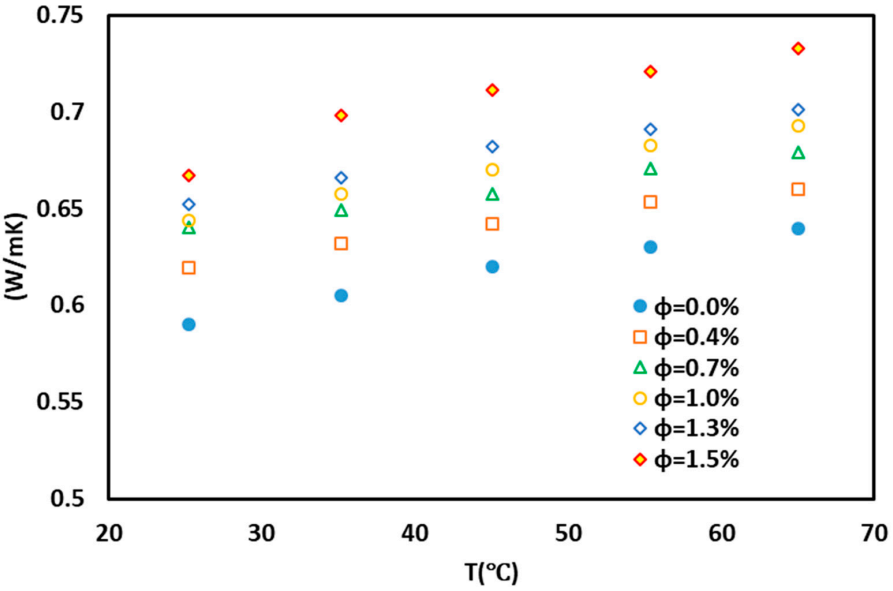

Figure 5. Variations in thermal conductivity coefficient of nanofluid with temperature and concentration of nanoparticles.

The relationships among the temperature, concentration, and thermal conductivity of the nanofluid were obtained on the basis of the experimental data. In Figures 5 and 6, the 3D contour illustrates the predicted data resulting from the experimental data. In the equations, x represents the concentration, y represents the temperature, and z is the thermal conductivity coefficient.

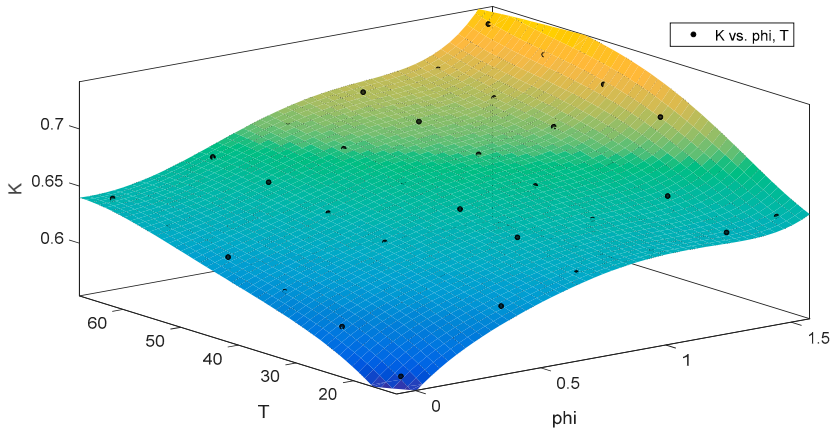

(a)

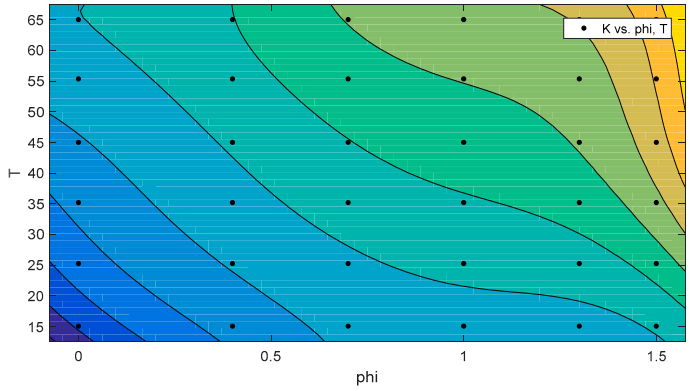

(b)

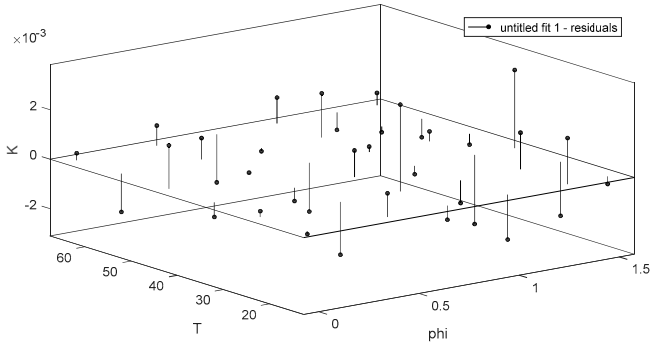

(c)

Figure 6. (**a**) Contour plots, (**b**) 3D, and (**c**) proposed model for the thermal conductivity coefficient (Temperature is in °C and phi (Volumetric Concentration (%)).

Linear model Poly55:

$$F(x, y) = p00 + p10 \times x + p01 \times y + p20 \times x^2 + p11 \times x \times y + p02 \times y^2 + p30 \times x^3 + p21 \times x^2 \times y + p12 \times x \times y^2 + p03 \times y^3 + p40 \times x^4 + p31 \times x^3 \times y + p22 \times x^2 * y^2 + p13 \times x \times y^3 + p04 \times y^4 + p50 \times x^5 + p41 \times x^4 \times y + p32 \times x^3 \times y^2 + p23 \times x^2 \times y^3 + p14 \times x \times y^4 + p05 \times y^5 \quad (2)$$

Coefficients (with 95% confidence bounds):

p10 = 3.494×10^{-1} (1.966×10^{-1}, 5.022×10^{-1})
p01 = 7.815×10^{-3} (-1.715×10^{-2}, 3.279×10^{-2})
p20 = -3.843×10^{-1} (-8.201×10^{-1}, 5.145×10^{-2})
p11 = -1.749×10^{-2} (-2.926×10^{-2}, -5.721×10^{-3})
p02 = -1.736×10^{-4} (-1.623×10^{-3}, 1.276×10^{-3})
p30 = 4.467×10^{-1} (-2.094×10^{-1}, 1.103)
p21 = 8.337×10^{-3} (-1.159×10^{-3}, 1.783×10^{-2})
p12 = 4.972×10^{-4} (7.729×10^{-5}, 9.171×10^{-4})
p03 = 1.163×10^{-6} (-3.839×10^{-5}, 4.071×10^{-5})
p40 = -3.24×10^{-1} (-7.665×10^{-1}, 1.186×10^{-1})
p31 = -4.751×10^{-3} (-1.065×10^{-2}, 1.146×10^{-3})
p22 = -4.931×10^{-5} (-2.011×10^{-4}, 1.025×10^{-4})
p13 = -7.265×10^{-6} (-1.401×10^{-5}, -5.195×10^{-7})
p04 = 1.758×10^{-8} (-4.95×10^{-7}, 5.302×10^{-7})
p50 = 8.486×10^{-2} (-2.493×10^{-2}, 1.946×10^{-1})
p41 = 2.198×10^{-3} (5.41×10^{-4}, 3.855×10^{-3})
p32 = -2.4×10^{-5} (-6.092×10^{-5}, 1.293×10^{-5})
p23 = 5.426×10^{-7} (-5.136×10^{-7}, 1.599×10^{-6})
p14 = 3.898×10^{-8} (-1.76×10^{-9}, 7.971×10^{-8})
p05 = -2.131×10^{-10} (-2.756×10^{-9}, 2.33×10^{-9})
p00 = 4.794×10^{-1} (3.199×10^{-1}, 6.388×10^{-1})

Figure 7 shows the effect of the increase of nanoparticles on the viscosity of the base fluid. As shown in Figures 7 and 8, as the nanofluid concentration increases, the viscosity increases. These solid particles in the base fluid increased the collision of particles, leading to an increase in viscosity. The equation and the corresponding graph for viscosity are presented below.

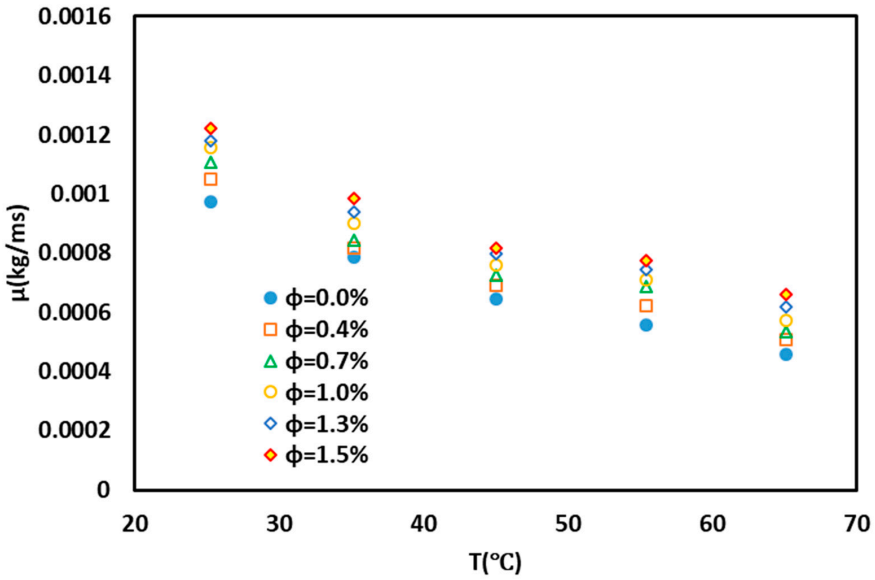

Figure 7. Viscosity variations of nanofluid with temperature and nanoparticle concentrations.

Linear model Poly55:

$$f(x, y) = p00 + p10 \times x + p01 \times y + p20 \times x^2 + p11 \times x \times y + p02 \times y^2 + p30 \times x^3 + p21 \times x^2 \times y + p12 \times x \times y^2 + p03 \times y^3 + p40 \times x^4 + p31 \times x^3 \times y + p22 \times x^2 \times y^2 + p13 \times x \times y^3 + p04 \times y^4 + p50 \times x^5 + p41 \times x^4 \times y + p32 \times x^3 \times y^2 + p23 \times x^2 \times y^3 + p14 \times x \times y^4 + p05 \times y^5 \quad (3)$$

Coefficients (with 95% confidence bounds):

p00 = 1.043×10^{-3} (1.442×10^{-4}, 1.941×10^{-3})
p10 = -1.066×10^{-4} (-9.675×10^{-4}, 7.544×10^{-4})
p01 = 4.699×10^{-5} (-9.37×10^{-5}, 1.877×10^{-4})
p20 = -5.178×10^{-4} (-2.973×10^{-3}, 1.937×10^{-3})
p11 = 4.561×10^{-5} (-2.071×10^{-5}, 1.119×10^{-4})
p02 = -3.333×10^{-6} (-1.15×10^{-5}, 4.832×10^{-6})
p30 = 4.982×10^{-4} (-3.198×10^{-3}, 4.195×10^{-3})
p21 = 2.274×10^{-5} (-3.076×10^{-5}, 7.625×10^{-5})
p12 = -2.283×10^{-6} (-4.649×10^{-6}, 8.235×10^{-8})
p03 = 6.58×10^{-8} (-1.57×10^{-7}, 2.886×10^{-7})
p40 = -2.457×10^{-4} (-2.739×10^{-3}, 2.248×10^{-3})
p31 = -1.03×10^{-5} (-4.352×10^{-5}, 2.292×10^{-5})
p22 = -3.773×10^{-7} (-1.233×10^{-6}, 4.781×10^{-7})
p13 = 4.347×10^{-8} (5.466×10^{-9}, 8.147×10^{-8})
p04 = -4.355×10^{-10} (-3.324×10^{-9}, 2.453×10^{-9})
p50 = 4.998×10^{-5} (-5.686×10^{-4}, 6.685×10^{-4})
p41 = 1.876×10^{-6} (-7.46×10^{-6}, 1.121×10^{-5})
p32 = 6.451×10^{-8} (-1.435×10^{-7}, 2.725×10^{-7})
p23 = 2.166×10^{-9} (-3.785×10^{-9}, 8.116×10^{-9})
p14 = -2.81×10^{-10} (-5.105×10^{-10}, -5.151×10^{-11})
p05 = 1.276×10^{-13} (-1.42×10^{-11}, 1.445×10^{-11})
Goodness of fit:
SSE: 2.306×10^{-9}
R-square: 0.9991
Adjusted R-square: 0.9979
RMSE: 1.24×10^{-5}

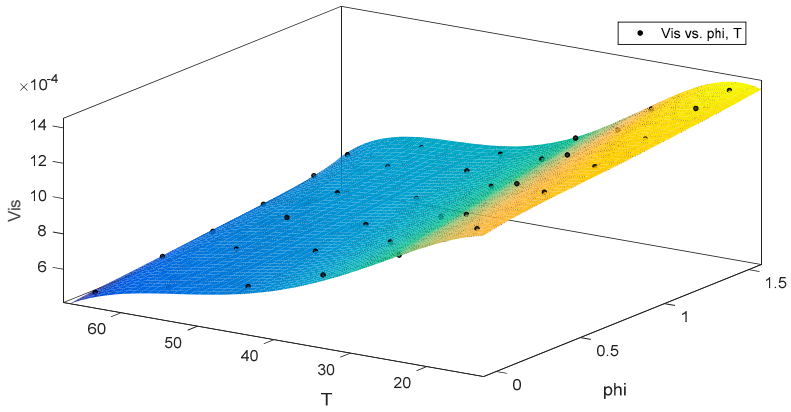

(a)

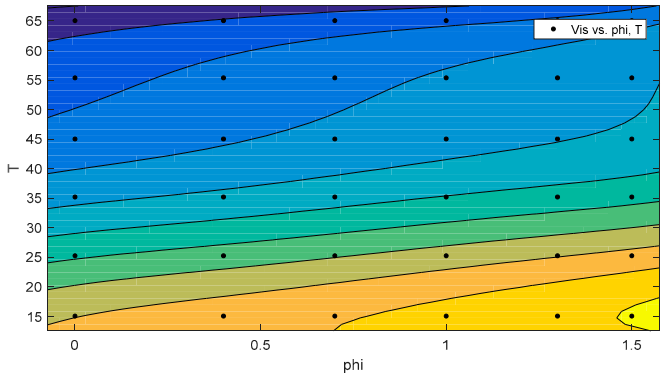

(b)

Figure 8. *Cont.*

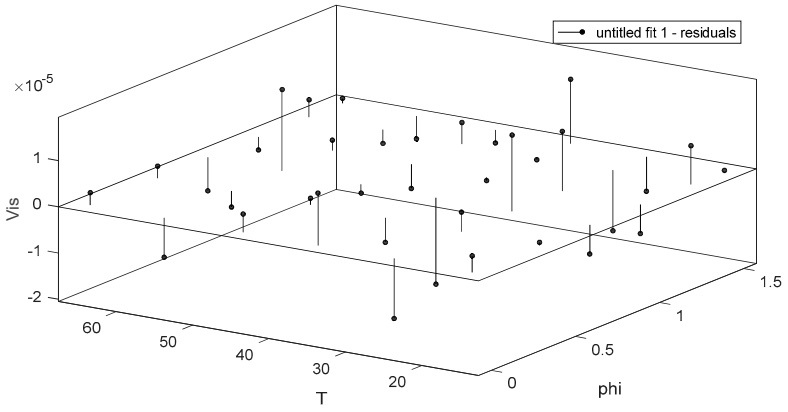

(c)

Figure 8. Contour graphs (3D) describing the model's (**a** to **c**) viscosity (Vis) distribution. (T (temperature) and phi (Volumetric Concentration (%)).

The data were obtained from the experiment that were necessary to find a favorable relation between output and input data, and these were the volumetric concentration and temperature of the fluid, respectively. Table 1 presents the range of each of these input parameters.

Table 1. Input parameters' range.

Parameter	Range
Temperature (°C)	10–70
Volumetric Concentration (%)	0.25–6

The nanofluid's thermal conductivity with respect to the base fluid is considered to be its thermal conductivity ratio, which is an appropriate measurement of nanoparticles with respect to thermal conductivity. As an illustration in SOM, competitive learning methods were developed based on particular properties of the human brain and were used for training. The arrangement of the human brain's cells in a distinct area is precise and meaningful. As an example, the sensory inputs of hearing or touch can contribute to an important geometric arrangement in distinct regions. Furthermore, processor units are located in nodes in SOM. By considering input patterns, units are arranged in a competitive learning approach. The units' position is arranged so that a useful coordinate system is created. Thus, a topographic map of the input patterns is created by the SOM in which units' position is associated with the input patterns' intrinsic characteristics. As illustrated in Figure 9, the base fluid's hexagonal arrangement leads to the prediction of the nanofluid's thermal conductivity ratio. The arrangement of the number of neurons is implemented in 9 × 9 shapes. The overall number associated with the neurons used is 81, with a neuron winner of 9 data. Thus, here, the neuron number 76 is the winner.

Radial basic networks are another kind of neural network. The comparison of baseline radius and post back networks indicates that the former requires a greater number of neurons, and the design of the latter requires more time. The performance of the former is exceptional under conditions in which there are very large educational vectors. Meanwhile, the input layer does not perform any processing. On the other hand, the hidden or second layer performs a significant part in converting nonlinear patterns to linear separation patterns. Finally, in order to find an approximation, a summation function with a linear output is produced by the third layer. Based on Figure 10, the correlation coefficient value was equal to 0.93875, which is auspicious.

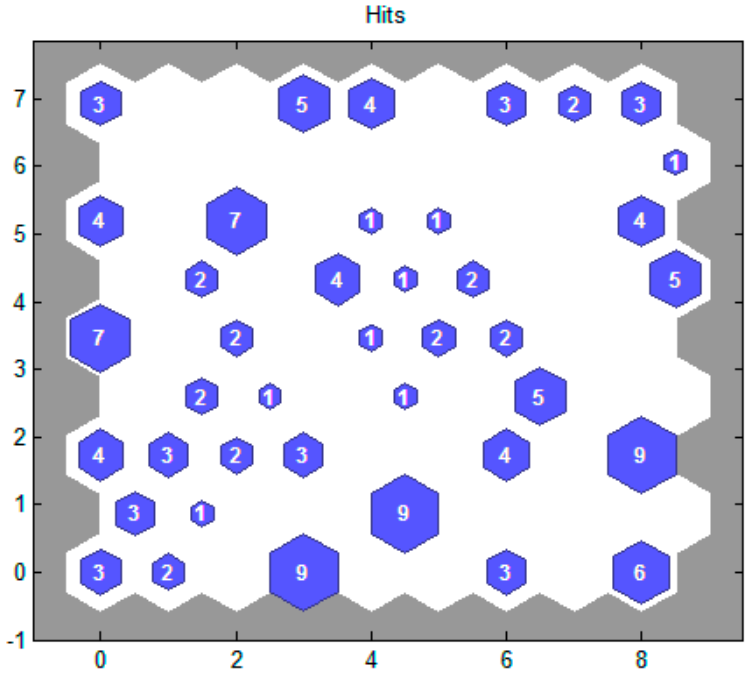

Figure 9. The structure of the neurons used and the quantity of assigned data.

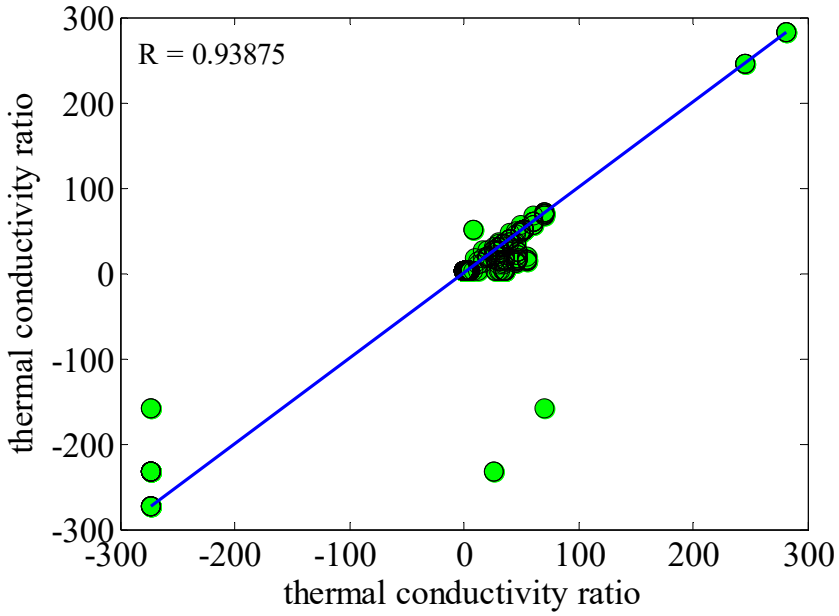

Figure 10. Correlation coefficient data based on investigating the predicted and experimental thermal conductivity ratio.

A BP-LM network training algorithm with a two-layered neural network was used for modeling. In this way, the nanoparticle size, volumetric concentration, and temperature were chosen as input data. Furthermore, the thermal conductivity ratio coefficient was employed as the target parameter. The sensitivity analysis is required for the number of neurons in the hidden layer. To achieve this purpose through application of the trial and error method, the quantity of neurons associated with the hidden layer was studied. As indicated in the Figure 10, the best performance belonged to the network with 76 neurons in the hidden layer. The reason for which numbers of neurons greater than 76 are not more attractive is that augmentation of the number of neurons increases the runtime as well as intensifying the possibility error in the model, even though exceptional outcomes are sometimes achieved by augmenting the number of neurons. According to Figure 11, the quantity of 0.98 expresses

the achieved correlation coefficient of the thermal conductivity ratio. The overall obtained data are placed within the circumference of the diameter line. The correlation coefficient can be enumerated as the most crucial predictive factor, such that better predictions can be made when this value is closer to 1. It can be clearly observed that the predicted and experimental data can be easily fitted, which is evidence of exceptionally favorable network prediction using 76 neurons.

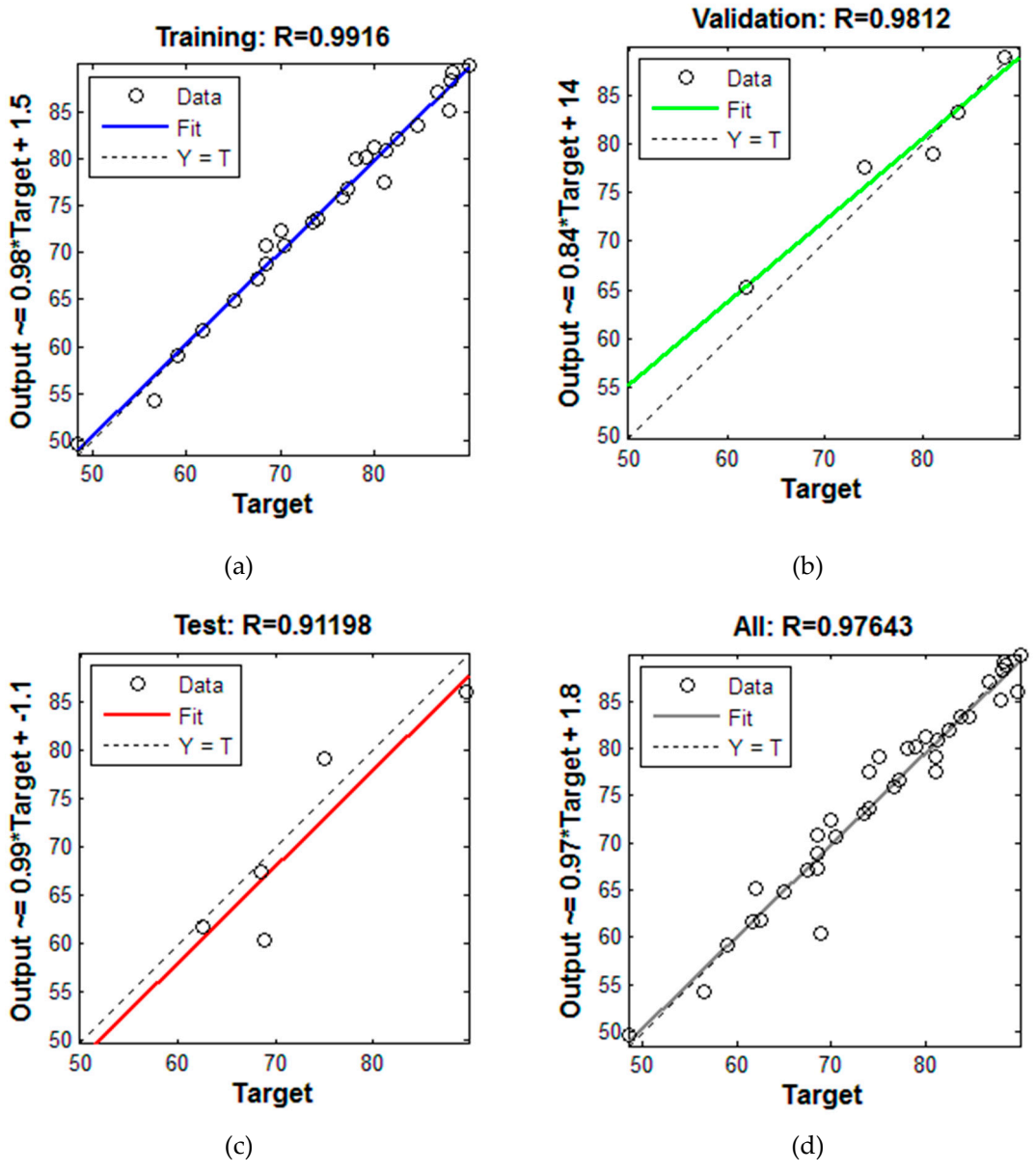

Figure 11. Results based on the correlation coefficient of thermal conductivity ratio. (**a**) Training, (**b**) Validation, (**c**) Test, (**d**) totally).

4. Conclusions

Firstly, the TiO_2-Al_2O_3 nanocomposite was synthesized. For the synthesis of nanocomposites, the sol–gel method and $TiCl_4$ and $AlCl_3$ compounds were used. The results of the analysis showed that all synthesized samples had dimensions in the nano range. After the synthesis of the nanocomposites, they were characterized by TEM. Adding alumina had a significant effect on the TiO_2 crystal size. The main reason for this is the formation of a homogeneous mixture of Ti-O-Al bonds during the sol–gel process. DSC (differential scanning calorimetry) was used to measure the specific heat capacity of the nanofluid. The nanocomposite showed a higher thermal capacity than its components at

300 K. A TC-Thermal Conductivity Analyzer (C-Therm Canada) was used to measure the thermal conductivity of the nanofluid-containing nanocomposite. The results showed that the average thermal conductivity was 11.7 W/mK. It should be noted that as the concentration of nanofluid increases, the agglomeration of particles also increases; as a result, the thermal conductivity of the nanofluid decreased. An increase in temperature also increases the thermal conductivity coefficient. Based on the experimental data, the relationships among concentration, temperature, thermal conductivity and viscosity were obtained. Finally, neural networks were used to predict the electrical properties of the nanofluid. For this purpose, a neural network with a multilayer perceptron structure was used to develop a model for estimating the thermal properties of nanofluids. In the end, the neural network was able to predict thermal properties by a correlation coefficient of 98%.

Author Contributions: Conceptualization, M.S., and H.M.; methodology, A.K.; writing—review and editing, M.G., M.H.A., A.M. and N.N.; supervision, M.H.A., A.M. and N.N.; Funding acquisition, A.M. and N.N. All authors have read and agreed to the published version of the manuscript.

Funding: This research is supported by the Hungarian State and the European Union under the EFOP-3.6.1-16-2016-00010 project and the 2017-1.3.1-VKE-2017-00025 project.

Acknowledgments: We acknowledge the support of the German Research Foundation (DFG) and the Bauhaus-Universität Weimar within the Open-Access Publishing Programme.

Conflicts of Interest: The authors declare no conflict of interest.

References

1. Ahmadi, M.H.; Ghazvini, M.; Alhuyi Nazari, M.; Ahmadi, M.A.; Pourfayaz, F.; Lorenzini, G.; Ming, T. Renewable energy harvesting with the application of nanotechnology: A review. *Int. J. Energy Res.* **2018**, *43*, 1387–1410. [CrossRef]
2. Ahmadi, M.H.; Ghazvini, M.; Baghban, A.; Hadipoor, M.; Seifaddini, P. Computing Approaches for Thermal C onductivity Estimation of CNT/Water Nanofluid. *Rev. des Compos. des Matériaux Avancés Soft* **2019**, *29*, 71–82. [CrossRef]
3. Ahmadi, M.H.; Baghban, A.; Sadeghzadeh, M.; Zamen, M.; Mosavi, A.; Shamshirband, S.; Kumar, R.; Mohammadi-Khanaposhtani, M. Evaluation of electrical efficiency of photovoltaic thermal solar collector. *Eng. Appl. Comput. Fluid Mech.* **2020**, *14*, 545–565. [CrossRef]
4. Sadeghzadeh, M.; Ahmadi, M.H.; Kahani, M.; Sakhaeinia, H.; Chaji, H.; Chen, L. Smart modeling by using artificial intelligent techniques on thermal performance of flat-plate solar collector using nanofluid. *Energy Sci. Eng.* **2019**, *7*, 1649–1658. [CrossRef]
5. Ahmadi, M.H.; Ghazvini, M.; Sadeghzadeh, M.; Alhuyi Nazari, M.; Kumar, R.; Naeimi, A.; Ming, T. Solar power technology for electricity generation: A critical review. *Energy Sci. Eng.* **2018**, *6*, 340–361. [CrossRef]
6. Shulepova, E.V.; Sheremet, M.A.; Oztop, H.F.; Abu-Hamdeh, N. Mixed convection of Al_2O_3–H_2O nanoliquid in a square chamber with complicated fin. *Int. J. Mech. Sci.* **2020**, *165*, 105192. [CrossRef]
7. Ahmadi, M.H.; Ghazvini, M.; Sadeghzadeh, M.; Alhuyi Nazari, M.; Ghalandari, M. Utilization of hybrid nanofluids in solar energy applications: A review. *Nano Struct. Nano Objects* **2019**, *20*, 100386. [CrossRef]
8. Nazari, M.A.; Ahmadi, M.H.; Sadeghzadeh, M.; Shafii, M.B.; Goodarzi, M. A review on application of nanofluid in various types of heat pipes. *J. Cent. South Univ.* **2019**, *26*, 1021–1041. [CrossRef]
9. Ahmadi, M.H.; Tatar, A.; Seifaddini, P.; Ghazvini, M.; Ghasempour, R.; Sheremet, M.A. Thermal conductivity and dynamic viscosity modeling of Fe_2O_3/water nanofluid by applying various connectionist approaches. *Numer. Heat Transf. Part A Appl.* **2018**, *74*, 1301–1322. [CrossRef]
10. Baghban, A.; Kahani, M.; Nazari, M.A.; Ahmadi, M.H.; Yan, W.-M. Sensitivity analysis and application of machine learning methods to predict the heat transfer performance of CNT/water nanofluid flows through coils. *Int. J. Heat Mass Transf.* **2019**, *128*, 825–835. [CrossRef]
11. Paluru, S.; Sudarsana Reddy, P.; Sheremet, M.A. A comparative study of Al_2O_3 and TiO_2 nanofluid flow over a wedge with non-linear thermal radiation. *Int. J. Numer. Methods Heat Fluid Flow* **2019**, *30*, 1291–1317.
12. Baghban, A.; Jalali, A.; Shafiee, M.; Ahmadi, M.H.; Chau, K.; Baghban, A.; Jalali, A.; Shafiee, M.; Ahmadi, M.H.; Chau, K.-W. Developing an ANFIS-based swarm concept model for estimating the relative viscosity of nanofluids. *Eng. Appl. Comput. Fluid Mech.* **2019**, *13*, 26–39. [CrossRef]

13. Maddah, H.; Aghayari, R.; Ahmadi, M.H.; Rahimzadeh, M.; Ghasemi, N. Prediction and modeling of MWCNT/Carbon (60/40)/SAE 10 W 40/SAE 85 W 90(50/50) nanofluid viscosity using artificial neural network (ANN) and self-organizing map (SOM). *J. Therm. Anal. Calorim.* **2018**, *134*, 2275–2286. [CrossRef]
14. Maddah, H.; Aghayari, R.; Mirzaee, M.; Ahmadi, M.H.; Sadeghzadeh, M.; Chamkha, A.J. Factorial experimental design for the thermal performance of a double pipe heat exchanger using Al_2O_3-TiO_2hybrid nanofluid. *Int. Commun. Heat Mass Transf.* **2018**, *97*, 92–102. [CrossRef]
15. Ahmadi, M.-A.; Ahmadi, M.H.; Fahim Alavi, M.; Nazemzadegan, M.R.; Ghasempour, R.; Shamshirband, S. Determination of thermal conductivity ratio of CuO/ethylene glycol nanofluid by connectionist approach. *J. Taiwan Inst. Chem. Eng.* **2018**, *91*, 383–395. [CrossRef]
16. Kahani, M.; Ahmadi, M.H.; Tatar, A.; Sadeghzadeh, M. Development of multilayer perceptron artificial neural network (MLP-ANN) and least square support vector machine (LSSVM) models to predict Nusselt number and pressure drop of TiO_2/water nanofluid flows through non-straight pathways. *Numer. Heat Transf. Part A Appl.* **2018**, *74*, 1190–1206. [CrossRef]
17. Baghban, A.; Pourfayaz, F.; Ahmadi, M.H.; Kasaeian, A.; Pourkiaei, S.M.; Lorenzini, G. Connectionist intelligent model estimates of convective heat transfer coefficient of nanofluids in circular cross-sectional channels. *J. Therm. Anal. Calorim.* **2018**, *132*, 1213–1239. [CrossRef]
18. Ahmadi, M.H.; Alhuyi Nazari, M.; Ghasempour, R.; Madah, H.; Shafii, M.B.; Ahmadi, M.A. Thermal conductivity ratio prediction of Al_2O_3/water nanofluid by applying connectionist methods. *Colloids Surfaces A Physicochem. Eng. Asp.* **2018**, *541*, 154–164. [CrossRef]
19. Nazari, M.A.; Ghasempour, R.; Ahmadi, M.H.; Heydarian, G.; Shafii, M.B. Experimental investigation of graphene oxide nanofluid on heat transfer enhancement of pulsating heat pipe. *Int. Commun. Heat Mass Transf.* **2018**, *91*, 90–94. [CrossRef]
20. Ramezanizadeh, M.; Ahmadi, M.H.; Nazari, M.A.; Sadeghzadeh, M.; Chen, L. A review on the utilized machine learning approaches for modeling the dynamic viscosity of nanofluids. *Renew. Sustain. Energy Rev.* **2019**, *114*, 109345. [CrossRef]
21. Rezaei, M.H.; Sadeghzadeh, M.; Alhuyi Nazari, M.; Ahmadi, M.H.; Astaraei, F.R. Applying GMDH artificial neural network in modeling CO_2 emissions in four nordic countries. *Int. J. Low Carbon Technol.* **2018**, *13*, 266–271. [CrossRef]
22. Ahmadi, M.H.; Sadeghzadeh, M.; Raffiee, A.H.; Chau, K. Applying GMDH neural network to estimate the thermal resistance and thermal conductivity of pulsating heat pipes. *Eng. Appl. Comput. Fluid Mech.* **2019**, *13*, 327–336. [CrossRef]
23. Ahmadi, M.H.; Baghban, A.; Sadeghzadeh, M.; Hadipoor, M.; Ghazvini, M. Evolving connectionist approaches to compute thermal conductivity of TiO_2/water nanofluid. *Phys. A Stat. Mech. Its Appl.* **2019**, *540*, 122489. [CrossRef]
24. Nasirzadehroshenin, F.; Sadeghzadeh, M.; Khadang, A.; Maddah, H.; Ahmadi, M.H.; Sakhaeinia, H.; Chen, L. Modeling of heat transfer performance of carbon nanotube nanofluid in a tube with fixed wall temperature by using ANN-GA. *Eur. Phys. J. Plus* **2020**, *135*, 217. [CrossRef]
25. Ahmadi, M.H.; Sadeghzadeh, M.; Maddah, H.; Solouk, A.; Kumar, R.; Chau, K. Precise smart model for estimating dynamic viscosity of SiO_2/ethylene glycol–water nanofluid. *Eng. Appl. Comput. Fluid Mech.* **2019**, *13*, 1095–1105. [CrossRef]
26. Hemmat Esfe, M.; Rostamian, H.; Esfandeh, S.; Afrand, M. Modeling and prediction of rheological behavior of Al_2O_3-MWCNT/5W50 hybrid nano-lubricant by artificial neural network using experimental data. *Phys. A Stat. Mech. Its Appl.* **2018**, *510*, 625–634. [CrossRef]
27. Hemmat Esfe, M.; Tatar, A.; Ahangar, M.R.H.; Rostamian, H. A comparison of performance of several artificial intelligence methods for predicting the dynamic viscosity of TiO_2/SAE 50 nano-lubricant. *Phys. E Low-dimensional Syst. Nanostructures* **2018**, *96*, 85–93. [CrossRef]
28. Hemmat Esfe, M.; Rostamian, H.; Reza Sarlak, M.; Rejvani, M.; Alirezaie, A. Rheological behavior characteristics of TiO_2-MWCNT/10w40 hybrid nano-oil affected by temperature, concentration and shear rate: An experimental study and a neural network simulating. *Phys. E Low Dimens. Syst. Nanostructures* **2017**, *94*, 231–240. [CrossRef]

29. Bahrami, M.; Akbari, M.; Bagherzadeh, S.A.; Karimipour, A.; Afrand, M.; Goodarzi, M. Develop 24 dissimilar ANNs by suitable architectures & training algorithms via sensitivity analysis to better statistical presentation: Measure MSEs between targets & ANN for Fe–CuO/Eg–Water nanofluid. *Phys. A Stat. Mech. Its Appl.* **2019**, *519*, 159–168.
30. Nafchi, P.M.; Karimipour, A.; Afrand, M. The evaluation on a new non-Newtonian hybrid mixture composed of TiO_2/ZnO/EG to present a statistical approach of power law for its rheological and thermal properties. *Phys. A Stat. Mech. Its Appl.* **2019**, *516*, 1–18. [CrossRef]
31. Mikhailenko, S.A.; Sheremet, M.; Öztop, H.; Abu-Hamdeh, N. Thermal convection in Al_2O_3-water nanoliquid rotating chamber with a local isothermal heater. *Int. J. Mech. Sci.* **2019**, *156*, 137–145. [CrossRef]
32. Vafaei, M.; Afrand, M.; Sina, N.; Kalbasi, R.; Sourani, F.; Teimouri, H. Evaluation of thermal conductivity of MgO-MWCNTs/EG hybrid nanofluids based on experimental data by selecting optimal artificial neural networks. *Phys. E Low Dimens. Syst. Nanostructures* **2017**, *85*, 90–96. [CrossRef]
33. Afrand, M.; Hemmat Esfe, M.; Abedini, E.; Teimouri, H. Predicting the effects of magnesium oxide nanoparticles and temperature on the thermal conductivity of water using artificial neural network and experimental data. *Phys. E Low Dimens. Syst. Nanostructures* **2017**, *87*, 242–247. [CrossRef]
34. Hemmat Esfe, M.; Nadooshan, A.A.; Arshi, A.; Alirezaie, A. Convective heat transfer and pressure drop of aqua based TiO_2 nanofluids at different diameters of nanoparticles: Data analysis and modeling with artificial neural network. *Phys. E Low Dimens. Syst. Nanostructures* **2018**, *97*, 155–161. [CrossRef]
35. Azizi, S.; Awad, M.M.; Ahmadloo, E. Prediction of water holdup in vertical and inclined oil–water two-phase flow using artificial neural network. *Int. J. Multiph. Flow* **2016**, *80*, 181–187. [CrossRef]
36. Azizi, S.; Ahmadloo, E.; Awad, M.M. Prediction of void fraction for gas–liquid flow in horizontal, upward and downward inclined pipes using artificial neural network. *Int. J. Multiph. Flow* **2016**, *87*, 35–44. [CrossRef]
37. Li, Y.; White, T.; Lim, S. Low-temperature synthesis and microstructural control of titania nano-particles. *J. Solid State Chem.* **2004**, *177*, 1372–1381. [CrossRef]
38. Li, B.; Wang, X.; Yan, M.; Li, L. Preparation and characterization of nano-TiO_2 powder. *Mater. Chem. Phys.* **2003**, *78*, 184–188. [CrossRef]
39. Zhang, R.; Gao, L. Preparation of nanosized titania by hydrolysis of alkoxide titanium in micelles. *Mater. Res. Bull.* **2002**, *37*, 1659–1666. [CrossRef]
40. Pavasupree, S.; Suzuki, Y.; Pivsa-Art, S.; Yoshikawa, S. Synthesis and characterization of nanoporous, nanorods, nanowires metal oxides. *Sci. Technol. Adv. Mater.* **2005**, *6*, 224–229. [CrossRef]
41. Colón, G.; Hidalgo, M.; Navío, J. A novel preparation of high surface area TiO_2 nanoparticles from alkoxide precursor and using active carbon as additive. *Catal. Today* **2002**, *76*, 91–101. [CrossRef]
42. Oliveira, M.; Machado, A.V. *Preparation of Polymer-Based Nanocomposites by Different Routes*; Portuguese Foundation of Science and Technology: Lisbon, Portugal, 2013.
43. Ghasemi, N.; Mirzaee, M.; Aghayari, R.; Maddah, H. Investigating Created Properties of Nanoparticles Based Drilling Mud. *Heat Mass Transf.* **2018**, *54*, 1381–1393. [CrossRef]
44. Ganguly, S.; Sikdar, S.; Basu, S. Experimental investigation of the effective electrical conductivity of aluminum oxide nanofluids. *Powder Technol.* **2009**, *196*, 326–330. [CrossRef]
45. Ahammed, N.; Asirvatham, L.G.; Wongwises, S. Effect of volume concentration and temperature on viscosity and surface tension of graphene–water nanofluid for heat transfer applications. *J. Therm. Anal. Calorim.* **2016**, *123*, 1399–1409. [CrossRef]
46. Toghraie, D.; Chaharsoghi, V.A.; Afrand, M. Measurement of thermal conductivity of ZnO–TiO_2/EG hybrid nanofluid. *J. Therm. Anal. Calorim.* **2016**, *125*, 527–535. [CrossRef]